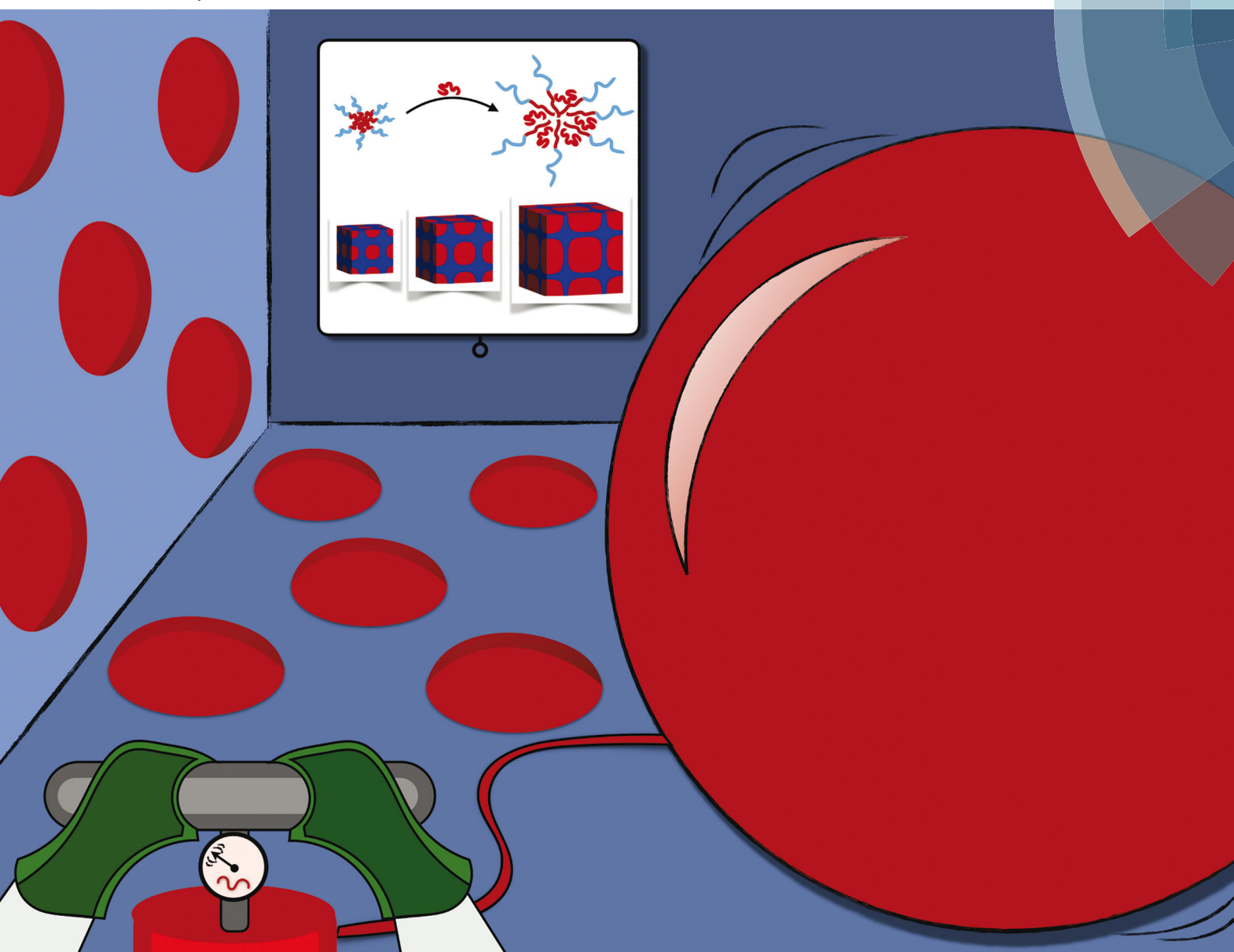
rsc.li/soft-matter-journal



ISSN 1744-6848



#### PAPFR



**View Article Online PAPER** 



Cite this: Soft Matter, 2019, **15**, 5193

Received 7th March 2019. Accepted 6th June 2019

DOI: 10.1039/c9sm00484j

rsc.li/soft-matter-journal

# Widely tunable persistent micelle templates via homopolymer swelling†

Amrita Sarkar, Akshay Thyagarajan, August Cole and Morgan Stefik \*\*D\*\*

The combination of precision control with wide tunability remains a challenge for the fabrication of porous nanomaterials suitable for studies of nanostructure-behavior relationships. Polymer micelle templates broadly enable porous materials, however micelle equilibration hampers independent pore and wall size control. Persistent micelle templates (PMT) have emerged as a kinetic controlled platform that uniquely decouples the control of pore and wall dimensions. Here, chain exchange is inhibited to preserve a constant template dimension (pore size) despite the shifting equilibrium while materials are added between micelles. Early PMT demonstrations were synthesis intensive with limited  $1-1.3 \times$  pore size tuning for a given polymer. Here we demonstrate PMT swelling with homopolymer enables  $1-3.2\times$ (13.3-41.9 nm) pore size variation while maintaining a monomodal distribution with up to 250 wt% homopolymer, considerably higher than the ~90 wt% limit found for equilibrating micelles. These swollen PMTs enabled nanomaterial series with constant pore size and precision varied wall-thickness. Kinetic size control here is unexpected since the homopolymer undergoes dynamic exchange between micelles. The solvent selection influenced the time window before homopolymer phase separation, highlighting the importance of considering homopolymer-solvent interactions. This is the first PMT demonstration with wide variation of both the pore and wall dimensions using a single block polymer. Lastly this approach was extended to a 72 kg mol<sup>-1</sup> block polymer to enable a wide 50-290 nm range of tunable macropores. Here the use of just two different block polymers and one homopolymer enabled wide ranging pore sizes spanning from 13.3-290 nm (1-22×).

## Introduction

The controlled fabrication of nanostructured porous materials is crucial for a wide variety of applications such as electrochemical energy conversion and storage devices. 1-16 Despite numerous developments with block polymer self-assembly, 1,6-8,17-21 access to fully tunable nanomaterials with independent control of pore and wall dimensions has remained elusive. 22,23 This challenge is often due to reliance upon equilibrium based approaches where each architectural dimension is fundamentally coupled to free energy minimization.<sup>24</sup> As with many polymer based strategies, a solid material is formed around the polymer from "material

Department of Chemistry & Biochemistry, University of South Carolina, Columbia, SC, USA. E-mail: morgan@stefikgroup.com

precursors" using a sol-gel reaction that results in a continuous solid ("walls", Scheme S1, ESI†). The subsequent removal of polymer, often via pyrolysis, results in the production of porosity where the polymer previously resided. With any such approach, further control of the polymer assembly improves the control over the material nanostructure. A kinetic controlled approach termed persistent micelle templates (PMT) was recently introduced to maintain a constant micelle dimension (pore template) and decouple the control of the wall thickness. 25,26 Here the micelle templates typically employ a hydrophilic corona block that preferentially interacts with the material precursors (sol), via e.g. hydrogen bonding. Thus the hydrophobic core of the micelle often serves as the template for porosity (Scheme S1, ESI†).25 With PMT the wall thickness is precisely tuned via the fraction of material precursors in the micelle solution. These material precursors are often water-reactive and change the water content of the solvent mixture, shifting the equilibrium micelle dimension with each material addition.<sup>25</sup> In contrast to dynamic micelles that change their size according to the equilibrium, persistent micelles maintain a constant size via kinetic entrapment.26 We note that tunable wall thickness was observed prior to PMT without consideration of kinetic control. 22,23,27-29 Kinetic micelle control is historically difficult to reproduce due to the lack of dynamic

<sup>†</sup> Electronic supplementary information (ESI) available: Schematic of swollen micelle used as a template, block polymer and homopolymer swelling experiment photographs, block polymer and homopolymer GPC elugrams, PMT SAXS model and fit parameters, swelled material template SAXS, and SEM images. See DOI: 10.1039/c9sm00484i

<sup>‡</sup> Present address: Department of Chemical & Biological Engineering, Rensselaer Polytechnic Institute, Troy, NY, USA.

<sup>§</sup> Present address: College of Engineering, Carnegie Mellon University, Pittsburgh,

Paper Soft Matter

chain exchange to erase the effects of the processing history. We recently found that ultrasonic cavitation can temporarily enable chain exchange between micelles that are otherwise kinetically trapped, 30,31 a step that is now included to improve the reproducibility of PMT procedures. 25,26,30,32,33 PMT nanomaterials follow model predictions<sup>25</sup> and have demonstrated angstrom-level precision tuning of wall-thickness.<sup>25</sup> To date, PMT has enabled tunable sample series spanning in pore size from 12-57 nm. While modest pore size tuning of 1-1.3× was demonstrated with individual polymers using switchable chain exchange mechanisms, 26,30,31 access to pore dimensions spanning wide ranges has thus far required the synthesis of multiple custom block polymers.

The expansion of micelle templates with swelling agents has been extensively investigated under conditions of equilibrium. Early works used low molar mass organic molecules as "pore expanders," including 1,3,5-trimethylbenzene, hexane, and other hydrocarbons. 34-38 A drawback of small molecule pore expanders is that the efficacy is reduced by their evaporation during film processing. Micelle template expansion with a swelling agent was first demonstrated with mesoporous silica.<sup>2,39-41</sup> Homopolymers have also been used as pore expanders by selectively swelling micelle cores. 29,42-44 A distinct advantage of homopolymers as pore expanders is that they are non-volatile. For example, a 1-1.6× increase in pore size was shown for polystyrene added to poly(styrene-b-ethylene oxide) templates for ordered mesoporous carbons. 42 Here, further addition of polystyrene homopolymer beyond 25-35% led to disordered and multimodal pore size distributions. A follow-up paper extended the same process to 87% homopolymer corresponding to a 1–2.06 $\times$ range of pore sizes. 43 Similarly, homopolymers have also been used to swell block polymer micelles without subsequent use as templates. 45 Lastly, homopolymers have been used to expand the feature sizes of bulk block polymers. 46-50 A general constraint was identified in the above works where the homopolymer molar mass is typically a fraction of that of the analogous polymer block (1:5 < molar mass ratio). Lastly, the body of literature focuses on systems under equilibration or with unknown kinetics. To the best of our knowledge the kinetic control of swollen micelle templates remains unstudied.

The known thermodynamics and kinetics of block polymer micelles provides a framework to develop swollen micelles with kinetic control. For block polymer micelles, the equilibrium diameter is the result of the balance between interfacial enthalpy (driving an increase in diameter to reduce surface area) and chain-stretching entropy (driving reduction in diameter to relax chain stretching), as well as other contributions. In contrast, the actual dimensions of a micelle depend on the history of shifting equilibrium conditions and the changing kinetics of chain exchange over time. The rates of chain exchange depend on the active mechanisms and the energetic barrier. For single chain exchange, the rate scales with a hypersensitive double exponent of  $\chi N$ , where  $\chi$  is the effective interaction parameter and N scales with the degree of polymerization of the core block. 51-59 Here the relevant  $\chi$  term is that between the core block and the solvent. Thus the use of a lower molar mass

homopolymer (lower N) naturally implies significantly faster exchange kinetics for the homopolymer as compared to the block polymer. Here we report the first PMT processing with widely tunable pore dimensions via micelle swelling with homopolymer. Kinetic control of the micelle dimension is shown to be possible despite apparent dynamic exchange of homopolymers between micelles. This approach enables the widest reported tuning of both pore size and wall thickness from a single block polymer.

# Experimental

#### **Materials**

Anhydrous, inhibitor free tetrahydrofuran (THF, 99%, Aldrich) and niobium(v) ethoxide (99.9%, Fisher) were stored inside a glove box and used as received. Ethanol (EtOH, 200 proof, 100%, Fisher) and methanol (MeOH, 99.8%, Fisher) were dried at room temperature by storing over 50% w/v of molecular sieves (3 Å, 8-12 mesh, Acros Organics) for a week. 60 37% w/w conc. HCl (ACS grade, VWR), poly(ethylene glycol)methyl ether (PEO-OH,  $M_n = 5000 \text{ g mol}^{-1}$ ,  $M_n = 20000 \text{ g mol}^{-1}$ , Aldrich), 2-bromopropionic acid (>99%, Aldrich), methyl-2-bromopropionate (99%, Aldrich), N,N'-dicylcohexylcarbodiimide (99%, Aldrich) and 4-(dimethylamino) pyridine (99%, Aldrich) were used as received. The ligand, tris-(2-dimethylaminoethyl) amine (Me<sub>6</sub>TREN) (97%, Aldrich) and catalyst, copper(1) bromide (99.99%, Aldrich) were stored inside a glove box and used as received. Hexyl acrylate (96%, VWR) monomer was passed through basic alumina column just before use. Chloroform (>99%, Aldrich), hexane (>98.5%, Fisher) and dimethylformamide (97%, Aldrich) were used as received.

#### Polymers synthesis and characterizations

Two poly(ethylene oxide-b-hexyl acrylate) diblock polymers were synthesized with different chain lengths and termed as OH1 and OH2. Both polymers were synthesized with a two-step procedure using a Steglich esterification followed by atom transfer radical polymerization (ATRP). These procedures were described elsewhere in detail.<sup>25</sup> Briefly, **OH1**  $(M_n 15 \text{k g mol}^{-1})$  and **OH2**  $(M_n = 72 \text{k g mol}^{-1})$  were synthesized from 5k and 20k g mol<sup>-1</sup> PEO-Br using a reagent ratio of [hexyl acrylate]: [PEO-Br]:  $[Me_6TREN]:[Cu(I)] = [200:1:0.5:0.5]$  and [700:1:0.5:0.5], respectively. Three cycles of freeze-pump-thaw (FPT) followed by backfilling of nitrogen were performed to ensure removal of oxygen from the reaction vessel. The OH2 polymerization reaction was carried out in DMF at 80 °C for 48 hours whereas for OH1 polymerized for 6 hours. A homopolymer poly(hexyl acrylate), termed H, was synthesized by ATRP using a reagent ratio of [hexyl acrylate]:[methyl-2-bromopropinoate]:[Me<sub>6</sub>TREN]:[Cu(I)] = 50:1:0.5:0.5. To a Schlenk flask, 307 μL of methyl-2-bromopropionate initiator was mixed with 22.7 mL of inhibitor free hexyl acrylate monomer. The flask was capped with a rubber septa, sealed tightened with copper wire and was sparged with nitrogen gas for 1 hour to remove oxygen. A catalyst stock solution of 1 mL of toluene containing 91 mg Cu(1)Br and 355 µL (0.5 mmol) Me<sub>6</sub>TREN ligand was prepared in a glovebox and

transferred via air-free syringe to the reaction flask under flowing N2 gas. This reaction mixture was placed into a preheated oil bath at 70 °C with constant stirring. The polymerization was conducted for 50 minutes. The reaction mixture was cooled before exposing the solution to air. The crude polymerization product was diluted with THF and passed twice through a basic alumina column to remove copper salts. The product was poured into 5-fold excess of cold methanol (-78 °C), using a dry iceacetone bath and the viscous homopolymer was washed three times with cold methanol. The collected polymer was dried using a rotovap and characterized by <sup>1</sup>H NMR and GPC. The molar mass of the PHA in block polymers was determined using a Bruker Avance III HD 300 <sup>1</sup>H NMR. <sup>1</sup>H NMR samples were prepared in CDCl<sub>3</sub>. The molar mass dispersity (D) was characterized by a Waters gel permeation chromatography (GPC) instrument equipped with a 515 HPLC pump, a 2410 refractive index detector, and three styragel columns (HR1, HR3 and HR4 in the effective molecular weight range of 0.1-5, 0.5-30, and 5-600 kg mol<sup>-1</sup>, respectively). THF was used as eluent at 30 °C temperature and with a flow rate of 1 mL minute<sup>-1</sup>. The GPC was calibrated with polystyrene standards (2570, 1090, 579, 246, 130, 67.5, 34.8, 18.1, 10.4, 3.4, 1.6 kg mol<sup>-1</sup>) obtained from Polymer Laboratories. GPC samples were prepared in THF with a concentration of 2–5 mg  $mL^{-1}$  and filtered through 0.2  $\mu m$ syringe filter just prior to injection.

#### Preparation of micelle templated materials

The micelle dispersion in alcohol (MeOH or EtOH) was prepared using 25 mg of dried block polymer (OH1 or OH2) and a prescribed amount of homopolymer (H) in 2.5 mL of dry solvent. These mixtures were heated to 50 °C until homogeneously dispersed, without visible polymer solids. This dispersion process took between 2-8 hours with the solution being checked every 30-40 minutes followed by brief manual agitation via shaking. When MeOH was the main solvent, the OH solutions appeared turbid after addition of H and did not clarify with longer heating or at higher temperature. In contrast, when EtOH was the main solvent, the OH solutions remained clear after addition of H. In both cases, the H gradually phase separated at RT (Fig. S1, ESI†). Then aqueous HCl was added dropwise to fresh solutions to make the total water content 2.0 wt%. The final solution in EtOH was sonicated for 5 minutes. Sonication was not performed with MeOH since that was found to expedite H phase separation. After water addition, a constant amount of Niobium Ethoxide ("material precursor") of 90 µL was added to examine the swollen micelle dimensions as a function of H loading. The time between acid addition and inorganic precursor addition was minimized to avoid water driven H phase separation. Each aliquot was spin coated for 20 seconds at 1000 rpm under 15%RH as described in detail elsewhere.25 Both glass coverslips and silicon wafers were used as substrates. These substrates were cleaned with freshly prepared piranha solution just prior to spin coating following procedure described in detail elsewhere.25 Immediately after spin coating, each sample was removed from the humidity-controlled chamber and placed on a hot plate for 15-20 minutes at 200 °C for coverslip glass and 8-12 hours at 100 °C for silicon substrates, respectively,

to crosslink the material, termed as "aging." The films were calcined in air (Barnstead Thermolyne muffle furnace) at 5 °C minute<sup>-1</sup> to 200 °C, then 15 °C minute<sup>-1</sup> to 550 °C with one hour hold, followed by natural cooling. The typical film thickness was between 400-600 nm.<sup>25</sup> The production of ample numbers of continuously tunable nanomaterials employing PMT condition were prepared via a one-pot titration approach 25,32 to vary the material to template (M:T) ratio. The M:T ratio was calculated as the mass ratio of final material (Nb<sub>2</sub>O<sub>5</sub>) relative to the total polymer mass (OH + H), assuming complete conversion of the oxide precursor.

#### **SEM** characterization

Top-view images of calcined films were acquired with a Zeiss Ultraplus thermal field emission SEM using an acceleration voltage of 5 keV using an in-lens secondary electron detector. The working distance was maintained at  $\sim 3$  mm as well as a constant magnification of 400k. Hundreds of measurements were made on each sample to yield statistically significant averages and statistical descriptors. It is well established that such evaporative processing followed by calcination lead to anisotropic film compression in the out-of-plane direction as the inorganic densifies. 26,61-65 Sample measurements were thus constrained in the in-plane dimensions to avoid these distortions. The wall-thickness was measured from the diameter of an inscribed circle drawn between micelles (Fig. S2, ESI†).33 The area of the inscribed circle was measured using ImageJ and the corresponding circle diameter was calculated from the reported circle area. Statistical metrics for pore and wall dimensions were determined by taking at least a hundred measurements on each sample. The mean value, the standard deviation, and the standard error of the mean were calculated. The standard error of the mean is equal to the standard deviation divided by  $\sqrt{N}$ , where N is the number of measurements. The mean values were reported plus or minus the standard error of the mean. The standard deviations were reported separately to indicate the numerical spread.

#### SAXS characterization

SAXS measurements were performed on spin coated films after an aging treatment. X-ray experiments were conducted using a SAXSLab Ganesha at the South Carolina SAXS Collaborative (SCSC). A Xenocs GeniX 3D microfocus source was used with a copper target to produce monochromatic beam with a 0.154 nm wavelength. The instrument was calibrated just before measurement, using the National Institute of Standards and Technology (NIST) reference material, 640c silicon powder with the peak position at  $2\theta = 28.44^{\circ}$ , where  $2\theta$  is the total scattering angle. A Pilatus 300k detector (Dectris) was used to collect the twodimensional (2D) scattering pattern with nominal pixel dimensions of 172  $\times$  172  $\mu m$ . The SAXS data were acquired with an X-ray flux of  $\sim 3.3$  M photon per second incident upon the sample and a sample-to-detector distance of 1040 mm. Transmission SAXS data were measured to observe the purely in-plane morphology. The 2D images were azimuthally integrated to yield the scattering

Paper

vector and intensity using SAXSGUI software. Peak positions were fitted using custom MATLAB software.

# Results and discussion

The design of an ideal PMT process with micelle swelling has several practical considerations. The swelling agent should be (1) non-volatile so that it maintains constant swollen micelle dimension throughout evaporative processing. The swelling agent should (2) selectively incorporate into only micelle cores for efficient size control and (3) phase separate from material precursors to avoid undesired secondary porosity<sup>32</sup> after calcination. These first 3 requirements are well met with a homopolymer of the same composition as the core block with a suitably lower molar mass. The processing solvent should be (4) capable of dispersing the desired micelles and have (5) limited solubility of the swelling agent. This last aspect makes micelle loading with swelling agent possible via temporary solvation and makes micelle loading preferential to swelling agent dissolution in the solvent phase. The processing solvent should also be (6) a poor solvent for the micelle core so that the solvent itself does not behave as a volatile swelling agent. Lower alcohols were found to satisfy requirements 4-6. Towards these ends, two poly(ethylene oxide-b-hexyl acrylate)s, OH1 and OH2 were prepared along with poly(hexyl acrylate) homopolymer (H) to examine pore expansion under kinetic control (Table 1 and Fig. S3, ESI†). The molar mass dispersity (D) of polymers prepared by ATRP can vary from 1.1-2.0 depending on the initiator activity, catalyst ratio, solvent content, trace contaminants, and extent of monomer conversion. 66-70 Following, prior guidelines for homopolymer swelling of equilibrating micelles, 42 the selected

H target had a  $\sim 4 \times$  lower molar mass with respect to the poly(hexyl acrylate) block in OH1.

### Homopolymer swelling of micelle templates in different alcohols

Pore size tuning was first examined using OH1 and H in MeOH. The H loading was varied from 0-500 wt% with respect to the OH1 mass. The MeOH based solutions were found to be metastable with the turbidity increasing gradually for several hours until complete phase separation of H after  $\sim 12$  hours, resulting in two clear phases (Fig. S1, ESI†). The effect of H loading upon the resulting pore dimensions was measured using SEM for direct measurements of pore size distributions (Fig. 1 and Table 2).

These data indicated that H addition led to monotonic expansion of the average pore size with monomodal pore size distributions up to a maximum of 250 wt% H, corresponding to a 1-2.3× pore size variation spanning from 15.7-35.7 nm (Fig. 2b and Table 2). Exceeding this loading with 500 wt% H led to a multimodal pore size distribution, presumably from a heterogeneous distribution of H within micelles or due to partial **H** phase separation from micelle cores (Fig. S4, ESI<sup>†</sup>).

In contrast, prior micelle template works under equilibration were generally limited to 87 wt% homopolymer loading before transition to multimodal foam-like pore size distribution. 42,43 For the present work, the gradual phase separation of H indicates that the micelles can be expanded beyond the equilibrium loading with a metastable time window sufficient to complete the templating process. The corresponding SAXS measurements exhibited a lattice expansion from 26.4 to 52 nm with H addition (Fig. 2a and Table 2). These data indicate a monotonic expansion of the correlation length, consistent with pore size expansion for

Table 1 Molecular characteristics of polymers

Samples	$M_{ m n,PEO}~({ m g~mol}^{-1})$	$M_{\mathrm{n,PHA}}^{a} (\mathrm{g \ mol}^{-1})$	Total $M_n^a$ (g mol <sup>-1</sup> )	Molar mass dispersity, $D^b$	$f_{\mathrm{PEO}}^{c}$	$f_{\mathrm{PHA}}{}^{c}$	Molar mass ratio: $M_{n,OH}: M_{n,H}$
Н	_	2400	2400	1.36	_	_	_
OH1	5000	10 000	15 000	1.17	0.33	0.67	4:1
OH2	20 000	51 000	71 000	1.60	0.28	0.72	21:1

<sup>&</sup>lt;sup>a</sup> Obtained from <sup>1</sup>H NMR. <sup>b</sup> Obtained from GPC analysis. <sup>c</sup> Volume fraction calculated using bulk densities, <sup>26,71</sup> PHA = 1.065 and PEO = 1.064 g cm<sup>-3</sup>.

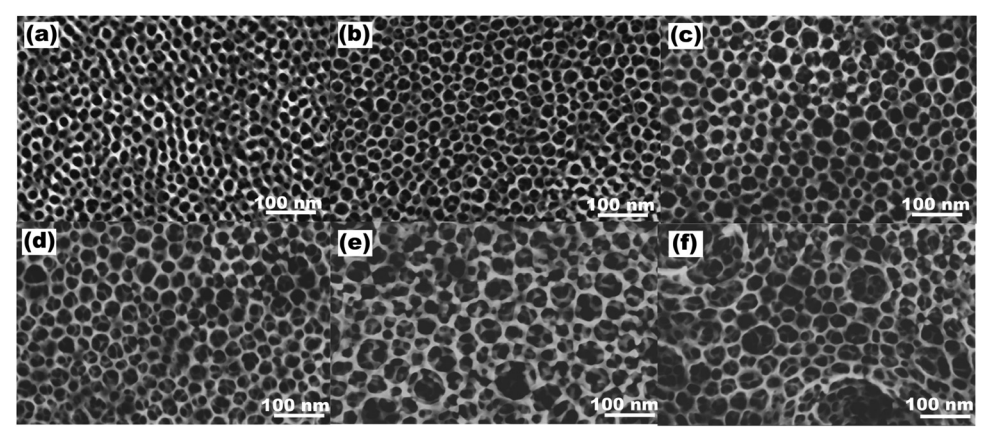


Fig. 1 SEM images of porous materials derived from swollen micelle templates as a function of homopolymer H loading: 0 wt% (a), 20 wt% (b), 80 wt% (c), 150 wt% (d), 250 wt% (e), and 500 wt% (f). The films were processed from MeOH using block polymer OH1 and homopolymer H

Soft Matter

Statistical measures of samples series prepared using OH1 + H in MeOH

H loading (wt%)	SEM average pore diameter $^{a,b}$ (nm)	Pore diameter standard deviation $(nm)$	SAXS <i>d</i> -spacing (nm)
0	$15.7 \pm 0.3$	3.2	26.4
20	$18.7\pm0.4$	3.9	29.6
80	$23.7 \pm 0.4$	3.9	37.1
150	$26.2 \pm 0.6$	5.6	41.1
250	$35.7 \pm 0.8$	7.9	47.4
500	$17.9 \pm 0.7^{c}$	2.8	52.0
	$28.8 \pm 0.5^{c}$	4.4	
	$41.6 \pm 0.4^{c}$	1.4	

<sup>a</sup> Mean value reported with  $\pm$  the standard error of the mean. <sup>b</sup> SEM and SAXS measurements were used to quantify in-plane sample dimensions. SAXS was performed on aged films and SEM was performed on calcined films. <sup>c</sup> Samples with multiple nominal pore sizes were subjected to the same quantification procedures after binning each measured value to one of the nominal distributions.

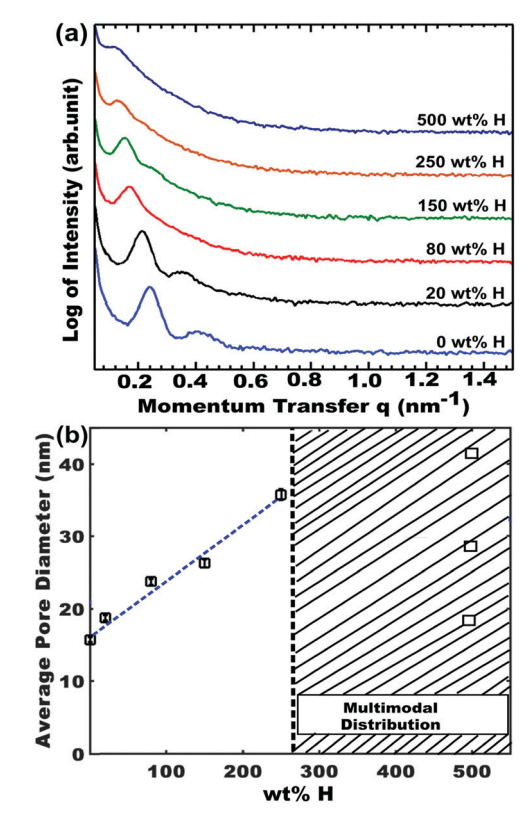


Fig. 2 SAXS data (a) and SEM pore dimensions (b) for materials prepared from swollen micelle templates as a function of homopolymer H loading. Error bars correspond to the error-of-the-mean. A trend line is presented in (b) to guide the eye. The films were processed from MeOH using block polymer OH1 and homopolymer H.

all H loadings up to 500 wt%. The SAXS patterns generally exhibited two peaks with an approximate q ratio of 1:2, for example 1:1.8 for OH1 with 0 wt% H (Fig. 2a). Similar structure factor peak ratios have been observed for randomly packed spherical micelles<sup>25,32</sup> and have been modeled with the Percus-Yevick effective hard sphere model. 72-74 SEM images also exhibited only short-range ordering that was consistent with a paracrystal. This limited short-range ordering is likely associated with the

dispersity of the micelle sizes, impeding organization into a simple lattice. The d-spacing from the first SAXS peak closely matched the mean SEM micelle-to-micelle spacing, which includes contributions from both the pores and walls (Table 2). Compared to prior works under equilibration, swollen micelle templates under kinetic-control, vide infra, enabled expanded homopolymer loading with a corresponding increased range of pore size tuning.

Homopolymer solubility in the processing solvent may reasonably be expected to play a role on the metastable time window for kinetic control. A closely related lower alcohol, EtOH, was next evaluated as the processing solvent. EtOH is slightly more hydrophobic than MeOH. In contrast, EtOH forms clear dispersions of OH1 + H that are stable for extended periods of at least 24 hours (Fig. S1, ESI†). A similar series of H loadings were evaluated using the same 2 wt% water and the same amount of material precursors. Owing to the more stable dispersion in EtOH, these micelles were homogenized using ultrasonic cavitation to induce chain exchange. 30,31 Similar to the above results, the micelle size was observed by SEM to monotonically expand up to 250 wt% H loading while preserving a monomodal pore size distribution (Fig. 3, 4b and Table 3).

The resulting average monomodal pore sizes spanned a broader range from 13.3-41.9 nm in EtOH, corresponding to a yet larger  $1-3.2 \times$  tuning range. This  $1-3.2 \times$  range of pore size tuning is considerably larger than prior demonstrations, e.g. showing 1-2.06× adjustment under equilibration. 43 Again, loadings exceeding 250 wt% H led to multimodal foam-like pore size distributions (Fig. 4c and Fig. S5, ESI†), where the solvent change significantly expanded the time window for metastable processing. Including the multimodal foam-like samples, the adjustable pore sizes spanned from 13.3-117 nm, corresponding to a 1-8.8× variation. This remarkably corresponds to nearly an order of magnitude in pore size tuning from a single block polymer. The compression ratio for the out-of-plane pore direction was calculated from measurements on cross-sectional SEM images of sample OH1 with 0 wt% H in EtOH. Here, the 6.1 nm mean out-ofplane size was 46% of the 13.3 nm mean in-plane pore size (Fig. S13, ESI†). Such distortions are ubiquitous in solution processed porous films from sol-gel chemistry. 25,26,32 The SAXS data with 0-250 wt% H loading led to a monotonic lattice expansion from 25.6-55.2 nm (Fig. 4a), and was consistent with the increasing nominal pore sizes. For a given homopolymer loading, the micelle dimensions were generally larger when processed from EtOH than from MeOH, with the exception of 0 wt% H. This general trend is counter to the expectations from  $\chi$  alone. When under kinetic control, the size of a micelle is determined both by thermodynamics as well as the kinetic trajectory from the processing history. The reproducible formation of kinetically trapped micelles is a broad challenge owing to the inherent lack of chain exchange processes. This equilibration challenge has likely hampered many prior efforts to realize reproducible kinetic control of micelles. We recently identified that ultrasonic cavitation is capable of temporarily enabling chain exchange between micelles that are otherwise kinetically trapped.30,31 Here ultrasonic cavitation was used to homogenize swollen micelles in EtOH only since the same process in MeOH led to H phase separation. Thus the samples processed from

Paper Soft Matter

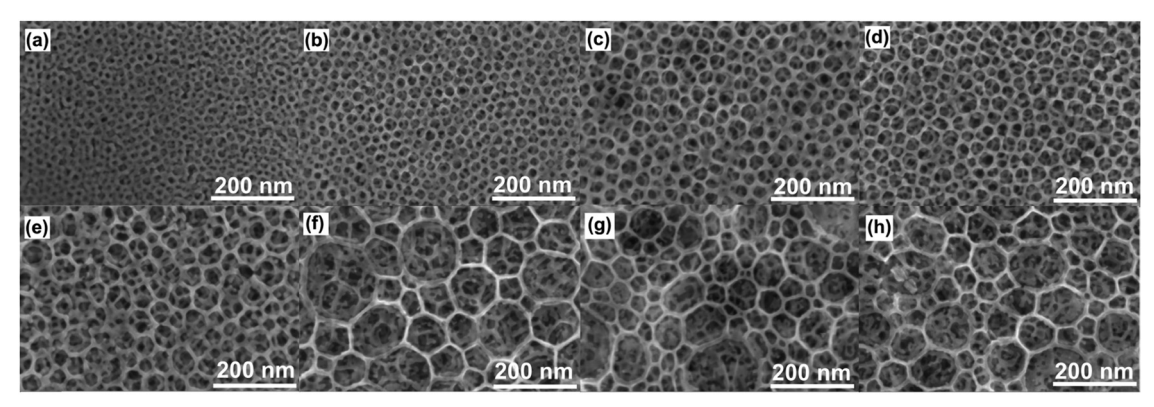


Fig. 3 SEM images of porous materials prepared from swollen micelle templates using EtOH. The films were prepared from OH1 with variable homopolymer H loading: 0 wt% (a), 20 wt% (b), 80 wt% (c), 150 wt% (d), 250 wt% (e), 500 wt% (f), 800 wt% (g) and 1000 wt% (h)

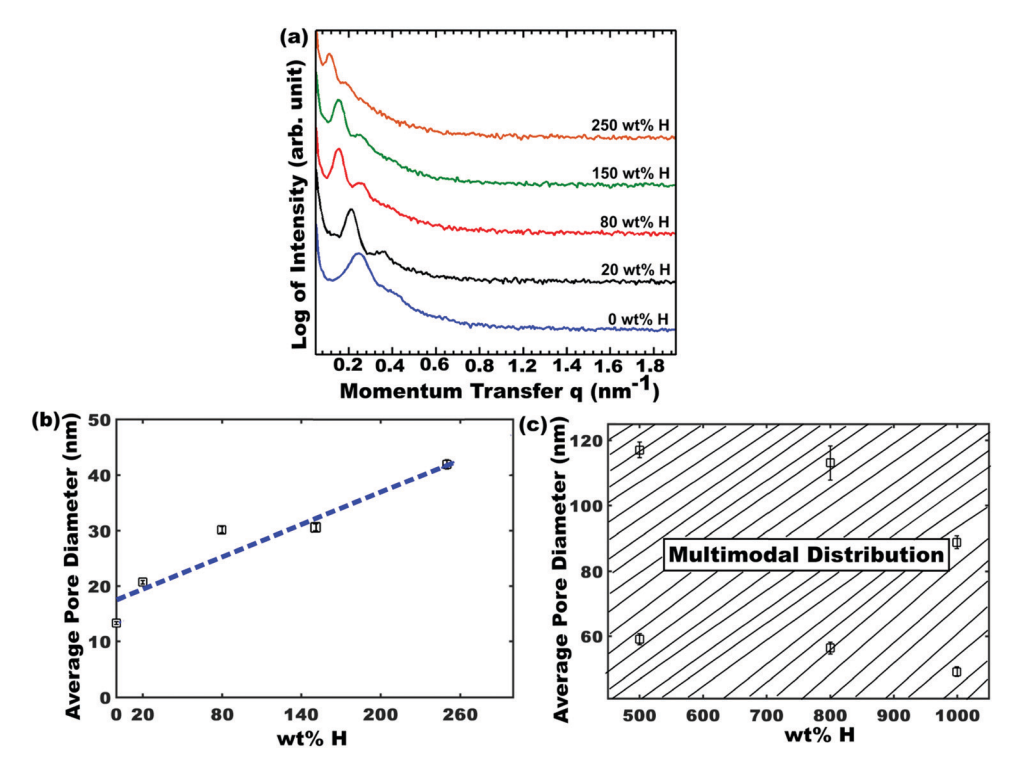


Fig. 4 SAXS data (a) and SEM pore dimensions (b and c) for templated materials prepared from OH1 in EtOH as a function of H loading. Error bars correspond to the error-of-the-mean. A trend line is presented in (b) to guide the eye.

MeOH are expected to vary more from batch to batch whereas the sample processed from EtOH are able to be homogenized with ultrasonic cavitation. An additional advantage of EtOH is that secondary pore formation within the walls was significantly suppressed as compared to MeOH (Fig. S6, ESI†). This feature is likely due to the enhanced removal of water with EtOH since it forms a low-boiling azeotrope with water whereas MeOH does not. EtOH was shown to enable a further improved range of micelle size tuning with greatly enhanced dispersion stability as compared to MeOH.

The significant difference in metastable time window warrants further discussion. Consider a solution of swollen persistent micelles, defined here as a condition where specifically the block polymer is not undergoing significant exchange between micelles, evidenced vida infra. Both MeOH and EtOH are relatively high-x solvents  $^{75-77}$  for poly(hexyl acrylate) *i.e.* poor solvents. However, the homopolymer is of much lower molar mass than the corresponding core block to facilitate micelle swelling, here a  $\sim 4 \times$  reduction of molar mass. Thus, the  $\chi N$  barrier for the homopolymer to exit the micelle core is correspondingly  $\sim 4 \times$ reduced compared to that of the block polymer. Measurements of micelle single chain exchange have noted a hypersensitivity to chain length where a minor 62% increase in chain length (N) led to a factor of 10 000× slower chain exchange kinetics, attributed to the double-exponential relationship of exchange rate to  $\chi N$ .<sup>51</sup> One should anticipate that the low-N H chains actively exchange

Statistical measures in samples series prepared using **OH1** + **H** in FtOH

H loading (wt%)	SEM average pore diameter <sup>a,b</sup> (nm)	Pore diameter standard deviation <sup>b</sup> (nm)	SAXS d-spacing <sup>b</sup> (nm)
0	$13.3 \pm 0.3$	2.8	25.6
20	$20.7 \pm 0.3$	3.3	29.8
80	$30.1 \pm 0.6$	6.0	41.1
150	$30.6 \pm 0.6$	5.8	40.8
250	$41.9\pm0.8$	8.4	55.2
500	$59.0 \pm 1.8^{c}$	14.5	d
	$117.1 \pm 2.4^{c}$	13.1	
800	$56.3 \pm 1.8^{c}$	17.6	d
	$113.0 \pm 5.2^{c}$	13.7	
1000	$49.1\pm1.4^{c}$	10.4	d
	$88.8 \pm 2.0^{c}$	13.4	

<sup>&</sup>lt;sup>a</sup> Mean value reported with  $\pm$  the standard error of the mean. <sup>b</sup> SEM and SAXS measurements were used to quantify in-plane sample dimensions. SAXS was performed on aged films and SEM was performed on calcined films. <sup>c</sup> Samples with multiple nominal pore sizes were subjected to the same quantification procedures after binning each measured value to one of the nominal distributions. d Peak of scattering intensity not observed.

between micelles. The observation of slow H phase separation is indicative of the homopolymer exiting micelle cores and aggregating in solution, leading to phase separation. If the H phase separation kinetics were solely determined by the rate at which homopolymers exit micelles, one would expect H to have a higher  $\gamma N$  barrier with MeOH than EtOH and thus have slower H phase separation in MeOH.<sup>32</sup> This is, however, the opposite of the observed behavior. Consider a homopolymer that leaves a micelle core and enters the solvent phase, it has multiple possible outcomes where it could (1) enter a different micelle core, (2) persist dissolved in solution (low solubility), or (3) aggregate with other homopolymer (phase separation). The relative probabilities of these outcomes will determine the time window for metastable processing. These considerations suggest that a key difference may reside with outcomes 2 or 3. Regarding outcome 2, EtOH is less of a poor solvent for H than MeOH so EtOH can thus likely tolerate a higher free-H concentration before solution saturation and subsequent phase separation. Regarding outcome 3, the re-dissolution of H aggregates is also a function of solvent quality. Each chain on an aggregate surface has a probability of re-entering the solution and subsequently undergoing the same 3 possible outcomes above. The enhanced process stability with EtOH was attributed to these considerations (higher H solubility, H re-dissolution) and highlights the impact of multiple intermolecular interactions upon micelle swelling.

#### Kinetic control of swollen micelle templates

We next examine the stability of swollen micelle templates towards the continued addition of material precursors. Equilibrating micelles are known to change both the micelle size (pore size) and the wall thickness during the addition of material precursors.<sup>25</sup> In contrast, persistent micelle templates have demonstrated series with constant pore size and variable wallthickness. 25,26,32,33 Such persistent micelle templates have not yet been examined with swollen micelles. We note that "persistent" in the present context is satisfied by a constant micelle template

dimension regardless of active homopolymer exchange. OH1 micelles were swollen with varying amounts of H and one-pot titrations<sup>25,32</sup> of material precursors were used to produce nanomaterial series. The resulting series were characterized by a combination of SAXS and SEM (Fig. 5 and Fig. S7, Table S1, ESI†). Again, the SAXS derived d-spacing values closely matched the mean micelle-to-micelle spacing measured by SEM, which includes contributions from both the pores and walls (Table S1, ESI†). EtOH was used as the solvent for the above-discussed benefits. A constant 3.5 wt% water was used for the 0 wt% and 60 wt% H series. However, this water content caused phase separation for 200 wt% H loading samples (Fig. S8, ESI†). An analogous 200 wt% H series were prepared with 1.8 wt% water and is included in Fig. 5. When micelle templates are persistent, they maintain a constant core size leading to constant pore size.26 The addition of material precursors thus leads to lattice expansion where the micelle separation increases to accommodate the extra volume and results in monotonically increasing wall thickness. Prior PMT reports identified the critical role of trace water content in preserving kinetic control of the nominal micelle size. 25,26,30,32,33 The subsequent addition of water-reactive material precursors gradually depletes this water reserve and lowers the thermodynamic barrier to chain exchange. In the present work, each addition of niobium ethoxide (Nb2O5 precursor) results in hydrolysis that consumes trace water from the micelle solution. Eventually a critical point is reached where there is insufficient water present to maintain kinetic control over the micelles. For a given recipe, this corresponds to PMT control until a critical upper limit for the material:template ratio. Thus the plots in Fig. 5 are only consistent with the PMT model when the micelles are persistent, deviations from this model suggest that micelles have undergone dynamic chain exchange. The general PMT analysis methods are next detailed, followed by discussion of the present data. Under PMT conditions, this lattice expansion normally leads to a line of slope 1/3 on a log-log plot of SAXS d-spacing vs. the material: template ratio.32 The log-log graph enables identification of consistency with PMT conditions independent of SEM measurements. The corresponding plot of SAXS d-spacing vs. material:template ratio can be modeled using a quasi-cube root model with input of the nominal pore size determined by SEM measurements.<sup>25</sup> The identified region of persistence is subsequently validated with independent and direct measurements of pore size distributions by electron microscopy. The wall-thickness within the persistent regime is also directly measured by SEM and compared to geometric model predictions and SAXS model interpretations. Applying these strategies, three different compositions, including 0 wt%, 60 wt% and 200 wt% were examined with one-pot material titrations (Fig. 5 and Table S1, ESI†). Since these series included very low M:T values, the approximations leading to the slope = 1/3 criteria were less accurate and thus the full PMT SAXS model was used on the log-log graphs, resulting in slight model curvature (Fig. 5a). For all sample series, the first scattering maxima monotonically shifted to lower q-spacing as additional material precursors were added, corresponding to monotonic lattice expansion (Fig. 5b and Fig. S9, ESI†). The entire series with 0 wt% H was consistent with persistent micelles for the examined range of M:T conditions.

Paper Soft Matter

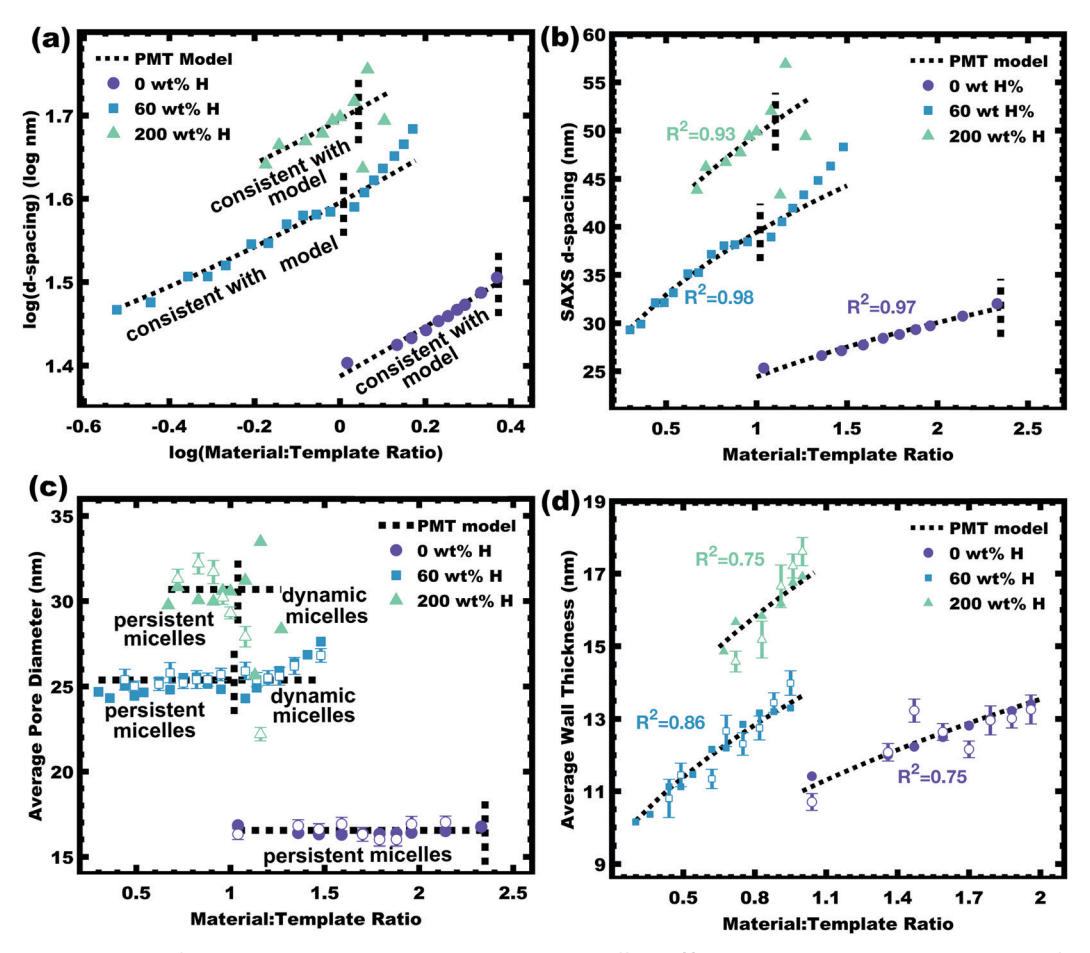


Fig. 5 Material titrations were performed with swollen micelle templates having different H loading. The material:template range of persistent micelle processing was determined by comparison to a quasi-linear log-log plot of the PMT model (a). The corresponding SAXS d-spacing trend resulted in a model best-fit (b). The best-fit model was used to determine the average pore size from the SAXS data and was compared to direct SEM measurements (c). The average wall thickness was compared similarly (d) SAXS data and model interpretations of SAXS data (closed symbols) are compared to direct SEM measurements (open symbols). The SEM values include the standard error-of-mean. These film series were processed from EtOH using block polymer OH1 and homopolymer H.

The 60 and 200 wt% H series were consistent with PMT conditions until critical M:T values of 1.02 and 1.04, respectively. The nominal pore size was determined for numerous samples within each PMT range and were used to refine best-fit values for the terms in a previously reported PMT SAXS model, using ESI† equations. The resulting best-fit lines for the 0, 60, and 200 wt% H samples had coefficient of determination  $(R^2)$  values of 0.97, 0.98, and 0.93, respectively, indicating strong agreements with the PMT model within the PMT window. The PMT windows were also validated by a second independent measurement pore size by direct observation via SEM (Fig. 5c and Fig. S7, Table S1, ESI†).

These SEM measurements supported that the micelle size was relatively constant within each PMT window. These data remarkably show the kinetic control of micelle templates that are swollen with homopolymer during the adjustment of the wall thickness. This feature is particularly curious in light of the apparent exchange of homopolymer chains throughout these processes, vide supra. Next, the average wall thickness was measured for each sample by SEM and compared with the dimension derived from the best-fit model interpretation of the

SAXS data, using ESI,† eqn (S3) (Fig. 5d). Each of the three PMT series, 0, 60, and 200 wt% H, exhibited good agreement between SEM and SAXS derived measurements as well as the PMT model. The coefficient of determination  $(R^2)$  values were 0.75, 0.86, and 0.75 for the 0, 60, and 200 wt% H series, respectively, indicating moderate agreement. The model fit parameters for all three compositions are presented in Table S2 (ESI†). All samples presented in Fig. 5 were prepared using a single block polymer, demonstrating the first independent and wide-ranging control of both pore size and wall thickness from a single block polymer.

#### Tunable macroporous materials via homopolymer swelling

The fabrication of well-controlled macroporous materials remains challenging from common block polymers. 16,26,78-80 Poly(styrene) and poly(methyl methacrylate) colloids are widely used to template macroporous materials (>50 nm), but are challenging to apply towards mesoporous materials (2-50 nm). 15,80-90 Studies of nanostructure-performance relationships span over many length scales for diverse materials and devices where ideally a single synthesis technique would enable granular adjustments of all architectural Soft Matter Paper

Table 4 Summary of measurements prepared by swelling OH2 with H

H loading (wt%)	SEM average pore diameter $^{a,b}$ (nm)	Pore diameter standard deviation (nm)	SEM average wall thickness $^{a,b}$ (nm)	Wall thickness standard deviation (nm)	SAXS d-spacing <sup>b</sup> (nm)
0	$49.6\pm0.9$	9.0	$22.1 \pm 0.7$	5.3	66.1
150	$76.3 \pm 1.5$	14.7	$26.3 \pm 1.1$	7.8	111.4
450	$156\pm4.5^{c}$	28.2	$29.0\pm1.1$	7.8	d
	$290 \pm 10.1^{c}$	25.6			

<sup>&</sup>lt;sup>a</sup> Mean value reported with  $\pm$  the standard error of the mean. <sup>b</sup> SEM and SAXS measurements were used to quantify in-plane sample dimensions. SAXS was performed on aged films and SEM was performed on calcined films. <sup>c</sup> Samples with multiple nominal pore sizes were subjected to the same quantification procedures after binning each measured value to one of the nominal distributions. d Peak of scattering intensity not observed.

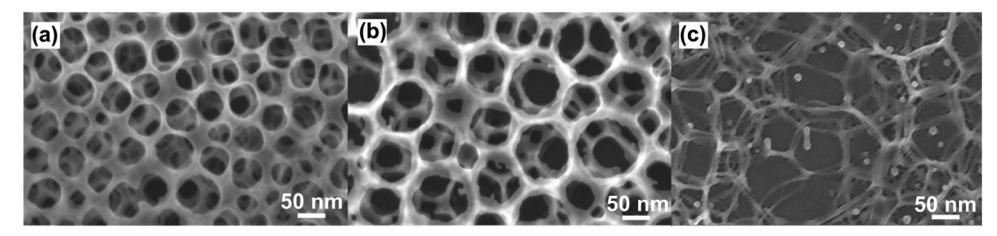


Fig. 6 SEM images of macroporous materials derived from a high molar mass block polymer OH2 as a function of homopolymer H loading: 0 wt% (a), 150 wt% (b), and 450 wt% (c),

features across orders of magnitude in length scale. The largest monomodal pore size achieved using OH1 with 250 wt% H was 41.9 nm, still within the limited regime of mesoporous materials. 81,88 Achieving monomodal macroporous distributions requires higher molar mass block polymers. 16,26 Towards this end, a higher molar mass block polymer OH2 was synthesized, having 72 kg mol<sup>-1</sup> (Table 1). The same H homopolymer (~21 times lighter than analogous PHA block in OH2) was used to assess pore size tuning in the macroporous regime. Monomodal pore size distributions from 49.6 to 76.3 nm were found with 0-150 wt% H, corresponding to 1–1.5 $\times$  range of pore size tuning (Table 4 and Fig. 6).

Higher homopolymer loadings resulted again in foam-like multimodal size distributions (Fig. S10, ESI†). The corresponding SAXS measurements exhibited lattice expansion from 66 to 111 nm, corresponding to 0-150 wt% H addition (Table 4 and Fig. S11, Table S3, ESI†). Such ultra-large nanostructures with thick walls pose a unique challenge towards achieving interconnected porosity via annealing (Fig. S12, ESI†). These data demonstrate that a small collection of just 2 block polymers with a homopolymer swelling agent can enable monomodal pore distributions tunable from 13.3-76.3 nm  $(1-5.7\times)$  and multimodal pore size distributions spanning from 13.3-290 nm (1-21.8×). Furthermore, these swollen micelles were shown to be compatible with PMT sample series having independent control over both the pore size and the wall thickness.

## Conclusions

Micelles swollen with homopolymers were shown to enable a significantly expanded range of size tuning when used under kinetic control as compared to equilibrium control. These swollen micelles were used as templates to demonstrate a wide 1-3.2× (13.3-41.9 nm) range of monomodal pore size tuning with a single block polymer. The processing solvent was found to have a significant impact on the metastable time window for swollen

micelle processing. Despite homopolymer exchange, the persistent micelle size enabled systematic nanomaterial series with constant pore size and variable wall thickness. The use of a higher molar mass block polymer enabled tunable monomodal macropores from 49.6-76.3 nm in diameter. This is the first PMT demonstration where both the pore size and wall thickness were independently tunable over wide ranges, here spanning more than an order of magnitude in pore size with two block polymers.

## Conflicts of interest

There are no conflicts to declare.

# Acknowledgements

A. S. acknowledges support from the National Science Foundation (DMR-1752615). M. S. acknowledges support by the National Science Foundation (DMR-1752615). This work made use of the South Carolina SAXS Collaborative. A. C. acknowledges financial support by the Summer Undergraduate Research Fund (SURF) at the University of South Carolina. We thank K. Lantz, Z. Marsh, B. Lamm and W. v. d. Bergh for the helpful discussions.

## Notes and references

- 1 P. Yang, D. Zhao, D. I. Margolese, B. F. Chmelka and G. D. Stucky, Nature, 1998, 396, 152-155.
- 2 D. Zhao, J. Feng, Q. Huo, N. Melosh, G. H. Fredrickson, B. F. Chmelka and G. D. Stucky, Science, 1998, 279, 548-552.
- 3 J. Wu, X. Liu and S. H. Tolbert, J. Phys. Chem. B, 2000, 104, 11837-11841.
- 4 S. Y. Choi, M. Mamak, N. Coombs, N. Chopra and G. A. Ozin, Adv. Funct. Mater., 2004, 14, 335-344.

Paper

D. Chen, Z. Li, Y. Wan, X. Tu, Y. Shi, Z. Chen, W. Shen, C. Yu,
 B. Tu and D. Zhao, J. Mater. Chem., 2006, 16, 1511–1519.

- 6 T. Brezesinski, J. Wang, J. Polleux, B. Dunn and S. H. Tolbert, *J. Am. Chem. Soc.*, 2009, **131**, 1802–1809.
- 7 G. A. Ozin, K. Hou, B. V. Lotsch, L. Cademartiri, D. P. Puzzo, F. Scotognella, A. Ghadimi and J. Thomson, *Mater. Today*, 2009, 12, 12–23.
- 8 M. Stefik, H. Sai, K. Sauer, S. M. Gruner, F. J. DiSalvo and U. Wiesner, *Macromolecules*, 2009, **42**, 6682–6687.
- 9 P. Docampo, S. Guldin, M. Stefik, P. Tiwana, M. C. Orilall, S. Huttner, H. Sai, U. Wiesner, U. Steiner and H. J. Snaith, *Adv. Funct. Mater.*, 2010, **20**, 1787–1796.
- 10 L. Song, D. Feng, N. J. Fredin, K. G. Yager, R. L. Jones, Q. Wu, D. Zhao and B. D. Vogt, ACS Nano, 2010, 4, 189–198.
- 11 M. Dai, L. Song, J. T. LaBelle and B. D. Vogt, *Chem. Mater.*, 2011, 23, 2869–2878.
- 12 P. Kohn, S. Pathak, M. Stefik, C. Ducati, U. Wiesner, U. Steiner and S. Guldin, *Nanoscale*, 2013, 5, 10518–10524.
- 13 C. Jo, J. Hwang, H. Song, A. H. Dao, Y.-T. Kim, S. H. Lee, S. W. Hong, S. Yoon and J. Lee, *Adv. Funct. Mater.*, 2013, 23, 3747–3754.
- 14 E. Kang, H. Jung, J.-G. Park, S. Kwon, J. Shim, H. Sai, U. Wiesner, J. K. Kim and J. Lee, ACS Nano, 2011, 5, 1018–1025.
- 15 M. Stefik, J. Song, H. Sai, S. Guldin, P. Boldrighini, M. C. Oriall, U. Steiner, S. M. Gruner and U. Wiesner, J. Mater. Chem. A, 2015, 3, 11478–11492.
- 16 K. Peters, H. N. Lokupitiya, D. Sarauli, M. Labs, M. Pribil, J. Rathousky, A. Kuhn, D. Leister, M. Stefik and D. Fattakhova-Rohlfing, Adv. Funct. Mater., 2016, 26, 6682–6692.
- 17 S. H. Tolbert, C. C. Landry, G. D. Stucky, B. F. Chmelka, P. Norby, J. C. Hanson and A. Monnier, *Chem. Mater.*, 2001, 13, 2247–2256.
- 18 X. Wang, C. Liang and S. Dai, Langmuir, 2008, 24, 7500-7505.
- 19 S. C. Warren, L. C. Messina, L. S. Slaughter, M. Kamperman, Q. Zhou, S. M. Gruner, F. J. DiSalvo and U. Wiesner, *Science*, 2008, 320, 1748–1752.
- 20 D. R. Dunphy, T. M. Alam, M. P. Tate, H. W. Hillhouse, B. Smarsly, A. D. Collord, E. Carnes, H. K. Baca, R. Köhn, M. Sprung, J. Wang and C. J. Brinker, *Langmuir*, 2009, 25, 9500–9509.
- 21 B. C. Garcia, M. Kamperman, R. Ulrich, A. Jain, S. M. Gruner and U. Wiesner, *Chem. Mater.*, 2009, 21, 5397–5405.
- E. Ortel, A. Fischer, L. Chuenchom, J. Polte, F. Emmerling,B. Smarsly and R. Kraehnert, *Small*, 2012, 8, 298–309.
- 23 D. Bernsmeier, E. Ortel, J. Polte, B. Eckhardt, S. Nowag, R. Haag and R. Kraehnert, *J. Mater. Chem. A*, 2014, **2**, 13075–13082.
- 24 US Department of Energy, Report of the Basic Energy Sciences Workshop on Basic Research Needs for Synthetic Science for Energy Relevant Technology, DOE Office of Science Tech. Rep. 1982.
- 25 A. Sarkar and M. Stefik, J. Mater. Chem. A, 2017, 5, 11840–11853.
- 26 H. N. Lokupitiya, A. Jones, B. Reid, S. Guldin and M. Stefik, Chem. Mater., 2016, 28, 1653–1667.
- 27 P. C. Angelome, M. C. Fuertes and G. J. A. A. Soler-Illia, Adv. Mater., 2006, 18, 2397–2402.

- 28 K. Nakanishi, Bull. Chem. Soc. Jpn., 2006, 79, 673-691.
- 29 L. Chuenchom, R. Kraehnert and B. M. Smarsly, *Soft Matter*, 2012, 8, 10801–10812.
- 30 H. N. Lokupitiya and M. Stefik, Nanoscale, 2017, 9, 1393-1397.
- 31 K. A. Lantz, A. Sarkar, K. C. Littrell, T. Li, K. Hong and M. Stefik, *Macromolecules*, 2018, 51, 6967–6975.
- 32 A. Sarkar, L. Evans and M. Stefik, *Langmuir*, 2018, 34, 5738–5749.
- 33 K. A. Lantz, N. B. Clamp, W. van den Bergh, A. Sarkar and M. Stefik, *Small*, 2019, 15, 1900393.
- 34 T. Kimura, Y. Sugahara, K. Kuroda and K. Kuroda, *Chem. Commun.*, 1998, 559–560.
- 35 A. Sayari, M. Kruk, M. Jaroniec and I. L. Moudrakovski, *Adv. Mater.*, 1998, **10**, 1376–1379.
- 36 J. L. Blin, C. Otjacques, G. Herrier and B.-L. Su, *Langmuir*, 2000, 16, 4229–4236.
- 37 M. Kruk and L. Cao, Langmuir, 2007, 23, 7247-7254.
- 38 M. Kruk, Acc. Chem. Res., 2012, 45, 1678-1687.
- 39 P. Schmidt-Winkel, W. W. Lukens, D. Zhao, P. Yang, B. F. Chmelka and G. D. Stucky, *J. Am. Chem. Soc.*, 1999, 121, 254–255.
- J. S. Lettow, Y. J. Han, P. Schmidt-Winkel, P. Yang, D. Zhao,
   G. D. Stucky and J. Y. Ying, *Langmuir*, 2000, 16, 8291–8295.
- 41 J. M. Kim, Y. Sakamoto, Y. K. Hwang, Y.-U. Kwon, O. Terasaki, S.-E. Park and G. D. Stucky, *J. Phys. Chem. B*, 2002, **106**, 2552–2558.
- Y. Deng, J. Liu, C. Liu, D. Gu, Z. Sun, J. Wei, J. Zhang, L. Zhang,
   B. Tu and D. Zhao, *Chem. Mater.*, 2008, 20, 7281–7286.
- 43 J. Wei, Y. Deng, J. Zhang, Z. Sun, B. Tu and D. Zhao, *Solid State Sci.*, 2011, **13**, 784–792.
- 44 J. Wei, Z. Sun, W. Luo, Y. Li, A. A. Elzatahry, A. M. Al-Enizi, Y. Deng and D. Zhao, *J. Am. Chem. Soc.*, 2017, **139**, 1706–1713.
- 45 M. D. Whitmore and T. W. Smith, *Macromolecules*, 1994, 27, 4673–4683.
- 46 D. J. Kinning, K. I. Winey and E. L. Thomas, *Macromolecules*, 1988, 21, 3502–3506.
- 47 K. I. Winey, E. L. Thomas and L. J. Fetters, *Macromolecules*, 1991, **24**, 6182–6188.
- 48 M. J. Greenall, D. M. A. Buzza and T. C. B. McLeish, *J. Chem. Phys.*, 2009, **131**, 034904.
- 49 Y. Li, J. Du and S. P. Armes, *Macromol. Rapid Commun.*, 2009, **30**, 464–468.
- 50 J. Wang, M. Muller and Z. G. Wang, *J. Chem. Phys.*, 2009, **130**, 154902.
- 51 S.-H. Choi, T. P. Lodge and F. S. Bates, *Phys. Rev. Lett.*, 2010, 104, 47802–47807.
- 52 L. Meli, J. M. Santiago and T. P. Lodge, *Macromolecules*, 2010, 43, 2018-2027.
- 53 S.-H. Choi, F. S. Bates and T. P. Lodge, *Macromolecules*, 2011, **44**, 3594–3604.
- 54 J. Lu, S.-H. Choi, F. S. Bates and T. P. Lodge, *ACS Macro Lett.*, 2012, **1**, 982–985.
- 55 J. Lu, F. S. Bates and T. P. Lodge, *ACS Macro Lett.*, 2013, 2, 451–455.
- 56 J. Lu, F. S. Bates and T. P. Lodge, *Macromolecules*, 2015, **48**, 2667–2676.

- 57 C. Sinturel, F. S. Bates and M. A. Hillmyer, ACS Macro Lett., 2015, 4, 1044-1050.
- 58 J. Lu, F. S. Bates and T. P. Lodge, Macromolecules, 2016, 49, 1405-1413.
- 59 Y. Ma and T. P. Lodge, Macromolecules, 2016, 49, 9542-9552.
- 60 D. B. G. Williams and M. Lawton, J. Org. Chem., 2010, 75, 8351-8354.
- 61 G. J. de, A. A. Soler-Illia and C. Sanchez, New J. Chem., 2000, 24, 493-499.
- 62 W. Ruland and B. M. Smarsly, J. Appl. Crystallogr., 2007, 40, 409-417.
- 63 J. Schuster, R. Kohn, A. Keilbach, M. Doblinger, H. Amenitsch and T. Bein, Chem. Mater., 2009, 21, 5754-5762.
- 64 T. Kimura, Y. Yamauchi and N. Miyamoto, Chem. Eur. J., 2010, 16, 12069-12073.
- 65 S. Dutta, K. C.-W. Wu and T. Kimura, Chem. Mater., 2015, 27, 6918-6928.
- 66 W. Tang and K. Matyjaszewski, Macromolecules, 2007, 40, 1858-1863.
- 67 J. Listak, W. Jakubowski, L. Mueller, A. Plichta, K. Matyjaszewski and M. R. Bockstaller, Macromolecules, 2008, 41, 5919-5927.
- 68 A. Plichta, M. Zhong, W. Li, A. M. Elsen and K. Matyjaszewski, Macromol. Chem. Phys., 2012, 213, 2659-2668.
- 69 V. Yadav, N. Hashmi, W. Ding, T.-H. Li, M. K. Mahanthappa, J. C. Conrad and M. L. Robertson, Polym. Chem., 2018, 9, 4332-4342.
- 70 X. Liu, C.-G. Wang and A. Goto, Angew. Chem., Int. Ed., 2019, 58, 5598-5603.
- 71 L. J. Fetters, D. J. Lohse, D. Richter, T. A. Witten and A. Zirkel, Macromolecules, 1994, 27, 4639-4647.
- 72 M. Schwab and B. Stuhn, Phys. Rev. Lett., 1996, 76, 924-927.
- 73 M. Schwab and B. Stuhn, Colloid Polym. Sci., 1997, 275, 341-351.

- 74 X. Wang, E. E. Dormidontova and T. P. Lodge, Macromolecules, 2002, 35, 9687-9697.
- 75 R. A. Orwoll, Rubber Chem. Technol., 1977, 50, 451-479.
- 76 O. Du, P. Hattam and P. Munk, *J. Chem. Eng. Data*, 1990, 35,
- 77 M. Tian and P. Munk, *J. Chem. Eng. Data*, 1994, 39, 742–755.
- 78 S. H. Park and Y. Xia, Chem. Mater., 1998, 10, 1745-1747.
- 79 M. C. Fuertes and G. J. A. A. Soler-Illia, Chem. Mater., 2006, 18, 2109-2117.
- 80 Y.-J. Cheng, L. Zhi, W. Steffen and J. S. Gutmann, Chem. Mater., 2008, 20, 6580-6582.
- 81 K. S. W. Sing, D. H. Everett, R. A. W. Haul, R. L. Moscou, R. A. Pierotti, J. Rouguerol and T. Siemieniewska, Pure Appl. Chem., 1985, 57, 603-619.
- 82 J. Rouquerol, D. Avnir, C. W. Fairbridge, D. H. Everett, J. H. Haynes, N. Pernicone, J. D. F. Ramsay, K. S. W. Sing and K. K. Unger, Pure Appl. Chem., 1994, 66, 1739-1758.
- 83 O. D. Velev and A. M. Lenhoff, Curr. Opin. Colloid Interface Sci., 2000, 5, 56-63.
- 84 Y. Xia, B. Gates, Y. Yin and Y. Lu, Adv. Mater., 2000, 12, 693-713.
- 85 A. Stein and R. C. Schroden, Curr. Opin. Solid State Mater. Sci., 2001, 5, 553-564.
- 86 G.-R. Yi, J. H. Moon and S.-M. Yang, Chem. Mater., 2001, 13, 2613-2618.
- 87 M. E. Turner, T. J. Trentler and V. L. Colvin, Adv. Mater., 2001, 13, 180-183.
- 88 G. J. de A. A. Soler-Illia, C. Sanchez, B. Lebeau and J. Patarin, Chem. Rev., 2002, 102, 4093-4138.
- 89 J. W. Long, B. Dunn, D. R. Rolison and H. S. White, Chem. Rev., 2004, **104**, 4463–4492.
- 90 Y.-J. Cheng, P. Muller-Buschbaum and J. S. Gutmann, Small, 2007, 3, 1379-1382.